Assigning mountain-valley fold lines of flat-foldable origami patterns based on graph theory and mixed-integer linear programming

Yao Chen [a,*], Linzi Fan [b], Yongtao Bai [c], Jian Feng [a], Pooya Sareh [d]

[a] Key Laboratory of Concrete and Prestressed Concrete Structures of Ministry of Education, and National Prestress Engineering Research Center, Southeast University, Nanjing 211189, China
[b] School of Civil Engineering, Sanjiang University, Nanjing 210012, China
[c] School of Civil Engineering, Chongqing University, Chongqing 400044, China
[d] Creative Design Engineering Lab (Cdel), School of Engineering, University of Liverpool, Liverpool, The Quadrangle, Brownlow Hill, L69 3GH, United Kingdom

A B S T R A C T

Traditional origami design is generally based on designers' artistic intuition and skills, mathematical calculations, and experimentations, which can involve challenges for crease patterns with a large number of vertices. To develop novel origami structures for engineering applications, systematic and easy-to-implement approaches capable of generating diverse origami patterns are desired, without requiring extensive artistic skills and experience in origami mathematics. Here, we present a computational method for automatically assigning mountain-valley fold lines to given geometric configurations of origami structures. This method is based upon a geometric-graph-theoretic representation approach combined with a graph-theoretic cycle detection algorithm, taking the subgraphs of a given structure as inputs. Then, a mixed-integer linear programming (MILP) model is established to find flat-foldable origami patterns under given constraints on the local flat-foldability and degree of vertices, leading to the identification of crease lines associated with local minimum angles. Numerical examples are presented to demonstrate the performance of the proposed approach for a range of origami structures with degree-4 or -6 vertices represented by their corresponding subgraphs.

1. Introduction

Origami – the centuries-old art of folding paper – is a highly creative, yet inexpensive, branch of art and design. Origami artists are skilled in turning a two-dimensional sheet of uncut paper [1] into an intricate three-dimensional object. Offering a diverse range of favorable functional properties, origami-inspired structures have been utilized in a wide variety of engineering applications in different scales, over the past few decades. Examples for such applications are deployable structures [2–5], energy-absorption structures [6–8], biomedical devises [9] and programmable metamaterials [10–13]. As a result, in order to further enrich origami theory and promote origami-inspired engineering applications, origami research has been of great importance to various scientific communities.

Recent study [14] has presented state-of-the-art reviews of the literature associated with the geometric modeling and design, folding kinematics, and structural analysis of origami-inspired struc-tures. In particular, the geometric design of novel origami pattern has garnered significant interest. Traditionally, to obtain a 3D configuration with expected geometric and physical properties, origami artists generally utilize their artistic intuition, experience, and trial and error processes to design appropriate crease patterns on a two-dimensional sheet [15]. Lang [16] introduced a series of mathematical methods and geometric techniques for the design generation of new origami crease patterns. Subsequently, Demaine et al. [15] presented geometric folding approaches for origami design. By using affine transformations and closed-loop equations, Belcastro and Hull [17] gave a numerical method for origami to expound the continuous rotations along the fold lines. Based on the basic constraints for a single degree-4 vertex (i.e., a four-fold node) of origami, Tachi [18] described a series of constraint equations for vertices and edges, and put forward a design method for rigid- and flat-foldable origami with quadrilateral facets. Based on given sets of vertices expressed in a Cartesian coordinate system, Zhou et al. [19] reported a numerical approach to developing three-dimensional origami structures. Qiu et al. [20] pointed out that origami structures could be simplified into equivalently redundant actuated mechanisms. Then, by using screw theory,

---

Wei and Dai [21] obtained new origami patterns from overconstrained mechanisms. Fuchi and Diaz [22] adapted a ground structure approach and a gradient-based search algorithm to developing possible 2 × 2 origami tessellations. Zimmermann and Stanković [23] established a sufficient and necessary condition for the rigid foldability of a degree-4 vertex in origami.

Although a series of analytical approaches to origami design have been presented, in general, designing new origami patterns may involve considerable analytical or computational challenges, especially for configurations with a large number of vertices [6]. Hence, systematic and easy-to-implement approaches that can effectively generate new origami patterns – without requiring extensive artistic skills and experience in origami mathematics – can be of great interest. Inspired by the ice-cracking process, McAdams and Li [24] employed the genetic algorithm to optimize origami patterns with flat-foldability. Since many origami structures contain remarkable periodicities or regularities [6], symmetry and regularity can be taken into consideration to simplify the origami design processes in many cases [25,26]. By performing a systematic symmetry reduction procedure while maintaining the flat-foldability of each vertex, Sareh and Guest [27] obtained symmetric derivatives of the Miura origami pattern and developed many descendants for this classic origami tessellation. Based on the definitions of undirected and directed graph products, Chen et al. [28] proposed an integrated geometric-graph-theoretic method for the mathematical representation of origami patterns. These computational design methods focus on the two-dimensional positions of vertices and edges to satisfy important folding properties such as flat-foldability and rigid foldability [18,29], where the mountain and valley folds are manually specified, or assumed to be known in advance. However, incorrect assignments on mountain and valley folds would not admit a flat folding of the obtained origami pattern (e.g., self-intersect in some way) [30], even if each vertex satisfies the flat-foldability. Thereafter, a completely automated and integrated design process for origami structures is expected, which should be capable of assigning valid mountain and valley folds for a general crease pattern.

Ehara and Kanno [31] utilized mixed-integer linear programming (MILP) and developed an effective platform to generate feasible connectivity patterns for a range of tensegrity structures under various constraints. Building up on their pioneering work, Xu et al. [32] incorporated more practical constraints for engineering applications, and further improved this approach to develop novel tensegrity structures.

Inspired by the usefulness of MILP in such structural form-finding problems, here we propose a computational method for automatically assigning valid mountain and valley folds of flat-foldable origami structures. The proposed approach exploits a geometric-graph representation and cycle detection using graph theory, combined with a mixed-integer linear programming model for pattern optimization. To effectively deal with the origami design problem, the degrees of vertices and independent subgraphs are taken as inputs, whilst edge lines are design variables. By imposing appropriate constraints on the degree and local flat-foldability of vertices, and positioning the fold lines associated with local minimum angles, optimal solutions for the edges and valid assignments for the fold lines can be identified.

Section 2 describes the fundamental theorems of flat-foldable origami, and introduces the graph-representation for origami structures. Section 3 establishes the optimization framework for origami design, and converts the original problem into a mixed-integral linear programming problem. Section 4 presents several examples to verify the automated mountain-valley assignment method for various origami structures. In Section 5, we discuss the applicability and computational efficiency of the proposed method.

2. Fundamentals of Flat-Foldable origami

2.1. Basic theorems for mountain-valley assignments

For a single-vertex crease pattern specified by a cyclic sequence α_1, α_2, ..., α_d of angles between successive crease lines around the degree-d vertex, the angles necessarily sum up to 360^0 in a flat piece of paper [15,33,34]. That is

$$\sum_{i=1}^{d} \alpha_i = 360°, \forall \alpha_i \in (0°, \ 180°). \tag{1}$$

The vertex is proven to be flat-foldable if and only if d is even and the sum of the even angles is identical to that of the odd angles [15,34], given by

$$\sum_{i=1}^{d/2} \alpha_{2i} = \sum_{i=1}^{d/2} \alpha_{2i-1} = 180°, \ \text{and d is even}. \tag{2}$$

Eqs. (1) and (2) provide the necessary condition for the local flat-foldability of each vertex in a two-dimensional origami crease pattern. Additionally, a valid mountain-valley assignment must be identified to allow the pattern to be flat-foldable. There are three basic theorems for assigning mountain and valley fold lines, as follows:

Theorem 1. *For a flat-foldable vertex intersected by mountain and valley fold lines, the number of valleys and that of mountains necessarily always differ by* ±2 [15,34].

Theorem 2. *On condition that an angle α_i is strictly smaller than its two neighboring angles, the two fold lines associated with angle α_i include one valley and one mountain. In other words,*

$$\{\alpha_i < \alpha_{i-1} \ and \ \alpha_i < \alpha_{i+1}\}$$
$$\Longleftrightarrow \alpha_i \ \text{is bounded by one valley and one mountain}. \tag{3}$$

Theorem 3. *If a total of $k < d$ equal angles $\alpha_i = \alpha_{i+1} = \cdots = \alpha_{i+k-1}$ are surrounded by strictly larger angles, given by*

$$\alpha_i = \alpha_{i+1} = \cdots = \alpha_{i+k-1} < \alpha_{i-1} \text{ and } \alpha_i = \alpha_{i+1} = \cdots = \alpha_{i+k-1}$$
$$< \alpha_{i+k}, \tag{4}$$

then, among the crease lines associated with these k angles for a flat-foldable single-vertex, the number of valley folds and that of mountain folds will be equal if k is odd, and will differ by ± 1 if k is even [15,26].

2.2. Graph representations of origami structures

In this section, an integrated geometric-graph-theoretic approach [28] is utilized to represent origami structures. An origami pattern can be neatly expressed by a specific graph G, which consists of a set of vertices **V**, a set of edges **E**, and a set of facets **F**. In general, a nodal coordinate vector should be associated with each vertex to exactly describe its location in the three-dimensional space. Additionally, an adjacency matrix $\mathbf{A}(G)$ is utilized to describe the adjacency and incidence for the vertices and edges of graph G (note that different types of origami structures can be expressed by directed or undirected graph products of independent graphs [28]). For instance, an origami pattern G with degree-4 ($d = 4$) vertices is the Cartesian product of subgraphs G_1 and G_2, i.e., $G = G_1 \gamma G_2$. Then, the adjacency matrix $\mathbf{A}(G_1 \gamma G_2)$ is written as

$$\mathbf{A}(G_1 \gamma G_2) = \mathbf{A}(G_1) \otimes \mathbf{I}_{G_2} + \mathbf{I}_{G_1} \otimes \mathbf{A}(G_2), \tag{5}$$

where $A(G_1)$ and $A(G_2)$ denote the adjacency matrices of the subgraphs G_1 and G_2, respectively, and $\otimes$ represents the Kronecker product of the matrices [35,36]. In Eq. (5), I_{G_1} and I_{G_2} are identity matrices, the dimensions of which are respectively equal to the dimensions of matrices $A(G_1)$ and $A(G_2)$.

It is known that the crease lines of a valid origami pattern will be either mountain folds (E_m), valley folds (E_v), or boundary edges (B). Thus, a valid origami crease pattern can be folded by assigning a partition of E into independent subsets

$$\mathbf{E} = \bar{\mathbf{E}} \cup \mathbf{B} = \mathbf{E_m} \cup \mathbf{E_v} \cup \mathbf{B}, \tag{6}$$

where $\bar{E}$ and B are the independent sets of internal and boundary edges, and $\cup$ denotes the union of the sets. Geometrically, each internal edge is always shared by two facets, while each boundary edge is owned by a single facet. Therefore, whether an edge j is a boundary edge can be evaluated by

$$\mathbf{j} \in \bar{\mathbf{E}} \iff |\mathbf{F}(\mathbf{j} \in \mathbf{E})| = 2, \tag{7}$$

and

$$\mathbf{j} \in \mathbf{B} \iff |\mathbf{F}(\mathbf{j} \in \mathbf{E})| = 1, \tag{8}$$

where $F(j \in E) \subseteq F$ denotes the set of indices of the facets connected to edge $j \in E$, and $|F(j \in E)|$ gives the number of independent facets connected to edge j. On condition that vertices V and the connectivity of edges (or $A(G)$) are given in advance, all facets F can be automatically detected, which is considered as a problem of finding a cycle in a sequence of iterated function values. For example, an n_F-sided facet F with n_F vertices $V_1, V_2, \ldots, Vn_F$ (and n_F edges) can be expressed as

$$F : V_1, \ V_2 = C(V_1), \ \cdots, \ V_{n_F} = C(V_{n_F-1}), \ \text{and} \ V_1 = C(V_{n_F}), \tag{9}$$

where $C(x)$ is a function associated with the vertices connected to a vertex x. In fact, detecting all the n_F-sided facets ($n_F > 2$) of a valid pattern is equivalent to counting the n_F-cycles of the graph G, which can be effectively found by existing cycle detection algorithms using graph theory [37–39].

In addition, $\bar{V}$ and V_b denote the sets of internal vertices and boundary vertices, respectively; we also have

$$V = \bar{V} \cup V_b \ \text{and} \ \bar{V} \cap V_b = \varnothing, \tag{10}$$

where the boundary vertices V_b can be obtained from the end points of the boundary edges. To further explain the graph representation of origami patterns and identification of boundary edges and vertices, Fig. 1 shows a classical Miura pattern G obtained from the Cartesian product ($G_1 \gamma G_2$) of two subgraphs G_1 and G_2. The path graph G_1 is a straight line with five vertices, and G_2 is a piecewise parallel polylines with five vertices.

As shown in Fig. 1, this origami pattern consists of 25 vertices, 40 edges, and 16 facets. The set of boundary edges B, evaluated from Eqs. (7) and (8), can be written as

$$\mathbf{B} = [1 \ 2 \ 3 \ 4 \ 5 \ 12 \ 14 \ 21 \ 23 \ 30 \ 32 \ 34 \ 36 \ 38 \ 39 \ 40]^{\mathrm{T}}. \tag{11}$$

Moreover, based on the nodal numbering of the vertices associated with the boundary edges, the set of boundary vertices V_b is given by

$$\mathbf{V}_b = [1 \ 2 \ 3 \ 4 \ 5 \ 6 \ 10 \ 11 \ 15 \ 16 \ 20 \ 21 \ 22 \ 23 \ 24 \ 25]^{\mathrm{T}}. \tag{12}$$

After obtaining the sets of boundary edges and vertices, mountain and valley folds can be assigned using the internal edges and vertices.

3. MILP-based optimization model

3.1. Integer variables for labelling fold lines

Recall that each edge of every facet in an origami pattern should belong to either E_m, E_v, or B. Here, to effectively assign mountain and valley folds, integer variables are adapted for labeling different kinds of fold lines. The label of a fold line j is denoted as

$$\mathbf{x}_j = \begin{cases} 1 & \text{if edge } j \text{ is a mountain fold} \\ -1 & \text{if edge } j \text{ is a valley fold} \\ 0 & \text{if edge } j \text{ is a boundary edge} \end{cases} \tag{13}$$

3.2. Objective functions

Besides flat-foldability, the convenience of manufacturing and efficient (or rigid) folding can be concerned during origami design. Designers generally use a seamless, relatively thin, sheet of material to be scored at certain fold lines, which is basically applicable to materials with sufficient ductility [26,27,40]. On the other hand, rigid facets (or frames with flexible membranes [41,42]) can be
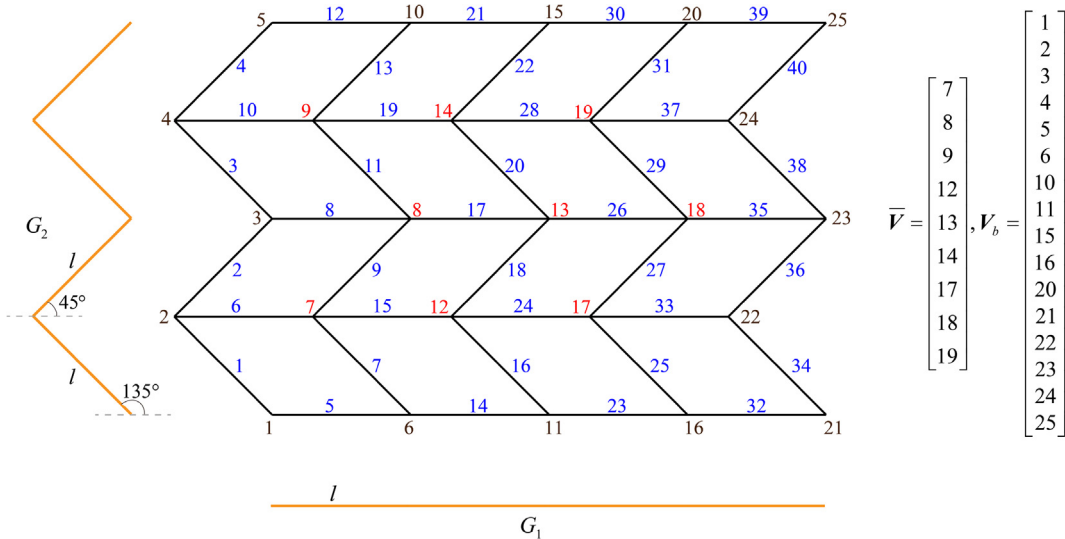

Fig. 1. Numbering of vertices and edges of a Miura fold pattern G represented by the Cartesian product ($G_1 \gamma G_2$) of two subgraphs G_1 and G_2.

neatly connected to each other using rotational hinges. In that case, the facets can be made of either ductile or brittle materials, provided that the origami structure is rigid-foldable.

To consider flat-foldable origami patterns with a small number of valley folds (or mountain folds), a linear objective function can be adopted, expressed as

$$f = -\sum_{j\in \boldsymbol{E}} \boldsymbol{x}_j \tag{14}$$

It is useful to introduce weighting coefficients to incorporate various factors in the final objective function. Then a new objective function f_η can be defined as

$$f_\eta = -\sum_{j\in \boldsymbol{E}} \eta_j \boldsymbol{x}_j \tag{15}$$

where η_j denotes the weighting coefficient for edge j. For instances, $\eta_j = l_j$ (edge length) can be used to minimize the length of valley folds in the final origami pattern. Note that similar objective functions can be formulated for a minimum number of mountain folds.

3.3. Constraints on mountain-valley assignments

First, by using the nodal coordinate vector and adjacency matrix of edges, angles at each vertex should be computed to evaluate the local flat-foldability condition for the given crease pattern. On condition that one or more vertices do not meet this condition (see Eqs. (1) and (2)), the geometric configuration has to be redesigned using a suitable origami design method [7,19]. To ensure that the assignment of mountain-valley folds satisfies the above-mentioned Theorem 1, each edge $j \in \boldsymbol{E}$ should satisfy

$$-2 \leqslant \sum_{j\in \boldsymbol{E}(i)} \boldsymbol{x}_j \leqslant 2, \quad \forall i \in \boldsymbol{V}, \tag{16}$$

where $\boldsymbol{E}(i) \subseteq \boldsymbol{E}$ denotes the set of indices of the edges connected to vertex $i \in \boldsymbol{V}$. Also, each degree-d vertex should satisfy

$$2 \leqslant \sum_{j\in \boldsymbol{E}(i)} |\boldsymbol{x}_j| \leqslant d, \quad \forall i \in \boldsymbol{V}. \tag{17}$$

Similarly, let us denote $\boldsymbol{E}_{\text{opposite}}(i) \subseteq \boldsymbol{E}$ as the set of the two opposite fold lines which are connected to vertex $i \in \boldsymbol{V}$ and associated with a local minimum angle α_i. Then, the basic constraint of Theorem 2 can be expressed as

$$\boldsymbol{x}_j + \boldsymbol{x}_{j'} = 0, \quad \forall (j,j') \in \boldsymbol{E}_{\text{opposite}}(i), \ and\ i \in \boldsymbol{V}. \tag{18}$$

For vertices with several local minimum angles, the additional constraint associated with Theorem 3 is established as

$$-1 \leqslant \sum_{j\in \boldsymbol{E}_{\text{equal}}(i)} \boldsymbol{x}_j \leqslant 1, \quad \forall i \in \boldsymbol{V}. \tag{19}$$

In addition, geometric constraints for the detected facets are necessary to be considered to ensure their adjacencies to the vertices and edges, given by

$$1 \leqslant |\boldsymbol{F}(i \in \boldsymbol{V})| \leqslant d \tag{20}$$

$$1 \leqslant |\boldsymbol{F}(j \in \boldsymbol{E})| \leqslant 2 \tag{21}$$

where $\boldsymbol{F}(i) \subseteq \boldsymbol{F}$ denotes the set of indices of the facets connected to vertex $i \in \boldsymbol{V}$, and $|\boldsymbol{F}(i \in \boldsymbol{V})|$ gives the number of independent facets connected to vertex i.

3.4. MILP formulation

It turns out that the original mountain-valley assignments of origami structures can be neatly formulated into a MILP problem, expressed as

$$\begin{aligned}
\underset{d,\ G,\ \boldsymbol{E},\ \boldsymbol{V}}{\text{minimize}}\ & f \\
\text{subject to}\ & x_j \in \{-1,\ 0,\ 1\}, \quad \forall j \in \boldsymbol{E} \\
& -2 \leqslant \sum_{j\in \boldsymbol{E}(i)} \boldsymbol{x}_j \leqslant 2, \quad \forall i \in \boldsymbol{V} \\
& 2 \leqslant \sum_{j\in \boldsymbol{E}(i)} |\boldsymbol{x}_j| \leqslant d, \quad \forall i \in \boldsymbol{V} \\
& \boldsymbol{x}_j + \boldsymbol{x}_{j'} = 0, \quad \forall (j,j') \in \boldsymbol{E}_{\text{opposite}}(i),\ i \in \boldsymbol{V} \\
& -1 \leqslant \sum_{j\in \boldsymbol{E}_{\text{equal}}(i)} \boldsymbol{x}_j \leqslant 1, \quad \forall i \in \boldsymbol{V} \\
& 1 \leqslant |\boldsymbol{F}(i \in \boldsymbol{V})| \leqslant d, \quad \forall i \in \boldsymbol{V} \\
& 1 \leqslant |\boldsymbol{F}(j \in \boldsymbol{E})| \leqslant 2, \quad \forall j \in \boldsymbol{E}
\end{aligned} \tag{22}$$

In Eq. (22), recall that $d \geqslant 4$ is the degree of the vertices, and G is the graph corresponding to the given configuration. In this MILP optimization model, only the even integer d, the nodal coordinates of vertices and the adjacency of edges are taken as inputs, which can be effectively evaluated from the graph representation of the origami pattern. Fig. 2 illustrates a brief flowchart associated with the exploited optimization process using graph theory and MILP. The proposed method is utilized to find flat-foldable origami structures with valid mountain-valley assignments, whereas feasible solutions can be optimized and the obtained origami patterns would be verified to be flat-foldable. To allow termination of re-design loop in the event that flat-foldability cannot be achieved, a termination condition for the number of loops t is denoted. The parameter $t_{\max}$ denotes the maximum number of iteration loops, and $t_{\max} = 100$ in this study.

4. Numerical examples

In this section, several numerical examples are presented to demonstrate the performance of the proposed method for the automated mountain-valley assignments of origami patterns. All the examples were implemented in MATLAB on a PC with an i7-8550U CPU@1.80 GHz and 16 GB of RAM.

4.1. Miura fold pattern

First, a simple Miura fold pattern, composed of a 5×5 array of vertices and 40 edges is investigated, as illustrated in Fig. 1. Recall that this Miura pattern can be expressed as the Cartesian product $G_1 \gamma G_2$ of subgraphs G_1 and G_2. Thus, the adjacency matrix $\mathbf{A}(G)$ can be directly computed by Eq. (5), that is

$$\begin{aligned}
\boldsymbol{A}(G_1 \square G_2) &= \boldsymbol{A}(G_1) \otimes \boldsymbol{I}_5 + \boldsymbol{I}_5 \otimes \boldsymbol{A}(G_2) \\
&= \begin{bmatrix} 0 & 1 & 0 & 0 & 0 \\ 1 & 0 & 1 & 0 & 0 \\ 0 & 1 & 0 & 1 & 0 \\ 0 & 0 & 1 & 0 & 1 \\ 0 & 0 & 0 & 1 & 0 \end{bmatrix} \otimes \boldsymbol{I}_5 + \boldsymbol{I}_5 \otimes \begin{bmatrix} 0 & 1 & 0 & 0 & 0 \\ 1 & 0 & 1 & 0 & 0 \\ 0 & 1 & 0 & 1 & 0 \\ 0 & 0 & 1 & 0 & 1 \\ 0 & 0 & 0 & 1 & 0 \end{bmatrix}.
\end{aligned} \tag{23}$$

Based on this adjacency matrix, a total of 16 quadrilateral facets are detected, where the automated cycle detection process using graph theory costs 0.0282 s. Subsequently, 9 internal vertices, 16 boundary vertices, 24 internal edges, and 16 boundary edges are identified. Note that the set of boundary edges has been given in Eq. (11), and the set of the internal fold lines can be written as

$$\bar{\mathrm{E}} = [6\ \ 7\ \ 8\ \ 9\ \ 10\ \ 11\ \ 13\ \ 15\ \ 16\ \ 17\ \ 18\ \ 19\ \ 20\ \ 22\ \ 24\ \ 25\ \ 26\ \ 27\ \ 28\ \ 29\ \ 31\ \ 33\ \ 35\ \ 37]^{\mathsf{T}}. \tag{24}$$
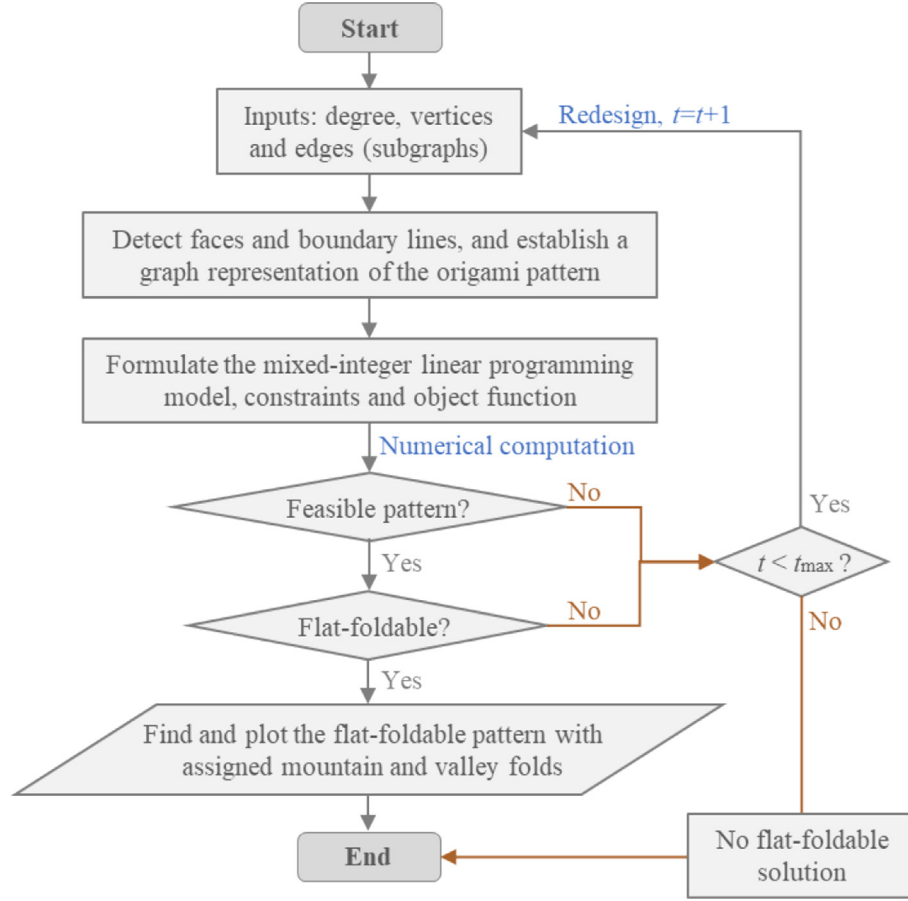
Fig. 2. Flowchart of the process of optimization based on graph theory and mixed-integer linear programing.

where the numbering of the edges is illustrated in Fig. 1. Each edge of the graph has an identical length (l), and the obtuse and acute angles between the first two vectors of subgraph G_2 and the X-axis (horizontal direction) are 135° and 45°, respectively. This given pattern is likely to be flat-foldable, as each vertex satisfies the necessary local flat-foldability in Eqs. (1) and (2).

To assign valid mountain or valley folds to internal edges, the lower and upper bounds for the variables are illustrated in parts (a) and (b) of Fig. 3. In this figure, red solid lines, blue dashed lines, and black bold lines represent mountain folds, valley folds, and boundary edges, respectively. Then, the 24-dimensional vectors $\boldsymbol{x}$ containing the integer variables for the internal fold lines shown in Fig. 3(a) and Fig. 3(b) are respectively given by
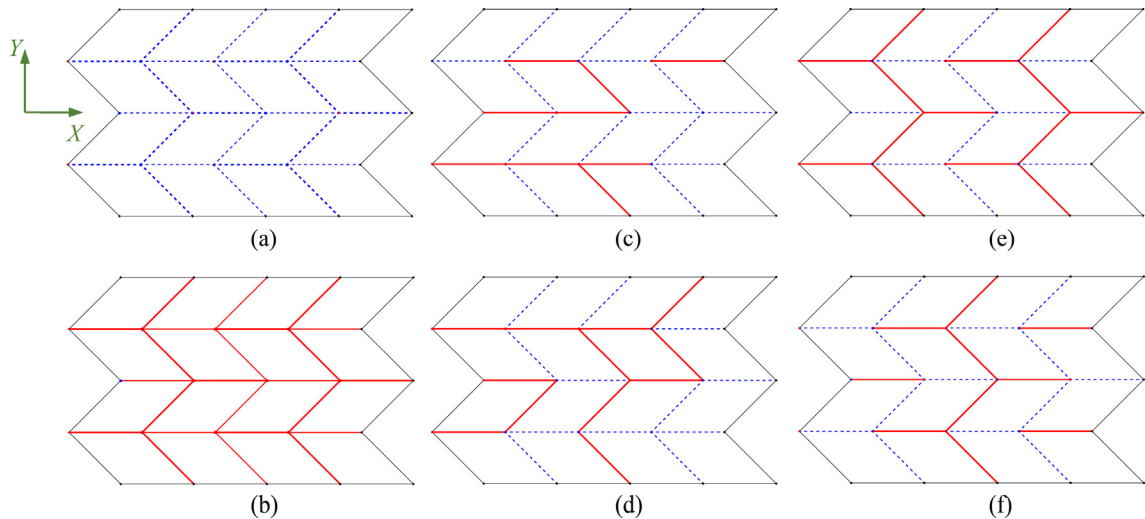

Fig. 3. Different mountain-valley assignments for a Miura geometric pattern with 5 × 5 vertices: (a) the lower bound for the edges ($j \in \boldsymbol{E}_v$); (b) the upper bound for the edges ($j \in \boldsymbol{E}_m$); (c & d) two random and invalid patterns; (e) the valid and flat-foldable pattern corresponding to the numerical solution; (f) equivalent (inverse) pattern for the numerical solution.

$$\boldsymbol{x}_{\text{lower}} = -[\,1 \quad 1\,]^{\text{T}}. \qquad (25)$$

$$\boldsymbol{x}_{\text{upper}} = [\,1 \quad 1\,]^{\text{T}}. \qquad (26)$$

Recall that the entry '-1' in Eq. (25) indicates a valley fold line, while the entry '1' in Eq. (26) indicates a monutain fold line. As the 24 internal edges can be potentially mountain or valley folds, the dimension of solution space reaches 2^{24}. For example, parts (c) and (d) of Fig. 3 show two random fold patterns for the given geometric design, where each internal edge is arbitrarily assigned to be a mountain or valley fold. Interestingly, using the proposed graph theory and MILP based approach, a feasible solution is found within 0.4145 s.

Fig. 3(e) illustrates the corresponding origami pattern with 14 mountain and 10 valley folds, where the numerical optimum solution obtained by the proposed algorithm is

$$\boldsymbol{x} = [\,1 \quad 1 \quad -1 \quad 1 \quad 1 \quad 1 \quad 1 \quad -1 \quad -1 \quad 1 \quad -1 \quad -1 \quad -1 \quad -1 \quad 1 \quad 1 \quad -1 \quad 1 \quad 1 \quad 1 \quad 1 \quad -1 \quad 1 \quad -1\,]^{\text{T}}. \qquad (27)$$

As expected, the obtained pattern has a minimum number of valley fold lines. This pattern shows regularity, and agrees well with the well-known mountain-valley assignments of the classical Miura fold pattern [7,19], verifying that the generated pattern is valid and flat-foldable. On the other hand, an equivalent (inverse) pattern with a minimum number of mountain folds can be found if the objective function given in Eq. (14) is modified as

$$\bar{f} = -f = \sum_{j \in \boldsymbol{E}} \boldsymbol{x}_j. \qquad (28)$$

The corresponding origami pattern has been depicted in Fig. 3 (f). It consists of 10 mountain folds and 14 valley folds, which are opposite to those of the pattern shown in Fig. 3(e).

4.2. Generalized degree-4 fold patterns

To further evaluate the performance of the proposed method for origami structures with generalized configurations or many vertices, two different patterns with 11×7 vertices are studied here. As shown in Fig. 4, both of them are generalized from a Miura pattern with a total of 77 vertices and 136 edges [27].

The subgraphs for describing the initial structure shown in Fig. 4(a) are characterized by the angles

$$\theta_{u1} = -10°, \theta_{u2} = 10°, \theta_{v1} = 120°, \text{ and } \theta_{v2} = 60°. \qquad (29)$$

where θ_{u1} and θ_{u2} denote the angles between the first two vectors of the horizontal subgraph and the X-axis, and θ_{v1} and θ_{v2} represent the angles between the bottom two vectors of the vertical subgraph and the X-axis. The lengths of the edges of the horizontal and vertical subgraphs are respectively l_u and l_v. Similarly, the subgraphs for describing the structure shown in Fig. 4(b) can be characterized by

$$\theta_{u1} = 0°, \theta_{u2} = 10°, \theta_{v1} = 115°, \text{ and } \theta_{v2} = 75° \qquad (30)$$

As can be seen from Fig. 4(b), the lengths of the adjacent edges of the horizontal subgraph are l_{u1} and l_{u2}, while the lengths of the adjacent edges of the vertical subgraph are l_{v1} and l_{v2}. Moreover, Fig. 4 demonstrates that each vertex satisfies the local flat-foldability, where the angles for typical vertices are given.

It costs 0.076 s and 0.0667 s to detect a total of 60 quadrilateral facets for the structures shown in Fig. 4(a) and (b), respectively. Each structure contains 32 boundary edges and 104 internal edges ($\bar{\boldsymbol{V}}$), and the dimensions of the involved edges sets $\boldsymbol{E}_{\text{equal}}$ and $\boldsymbol{E}_{\text{opposite}}$ are 45. Based on the detected edges, optimal solutions for both structures are obtained, where the corresponding computations cost 0.6335 s and 0.6692 s, respectively. The optimized assignments of mountain and valley folds are shown in Fig. 5.

It turns out that each pattern is composed of 57 mountains and 47 valleys, showing strong regularity. Although the locations of the
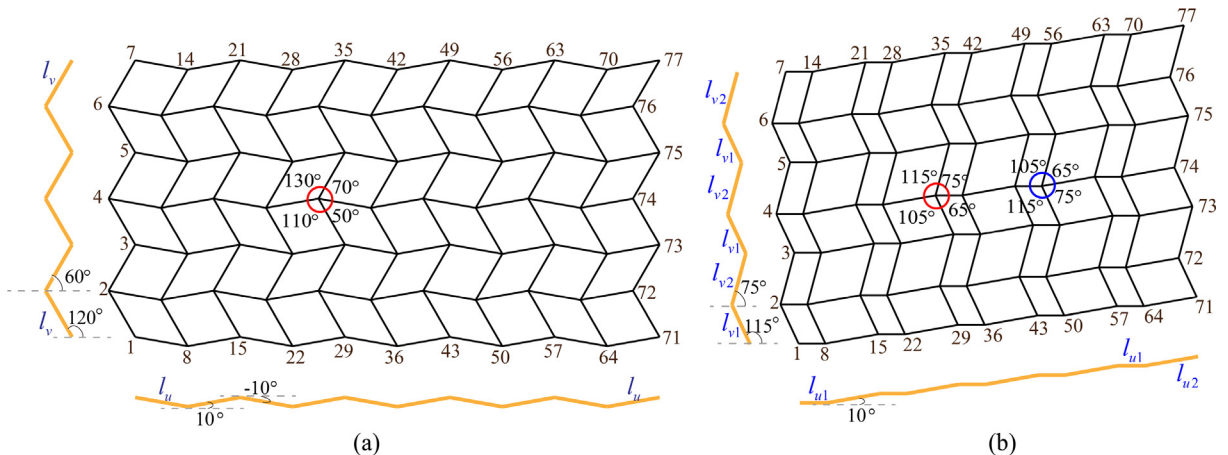

Fig. 4. Symmetric descendants of the Miura-ori with 11×7 vertices represented by the Cartesian product of their corresponding subgraphs: (a) a $pgg_{2,2}^{+}$ descendant with edges with identical lengths; (b) a $(p2)_{2,2}^{+}$ descendant with edges with two different lengths.
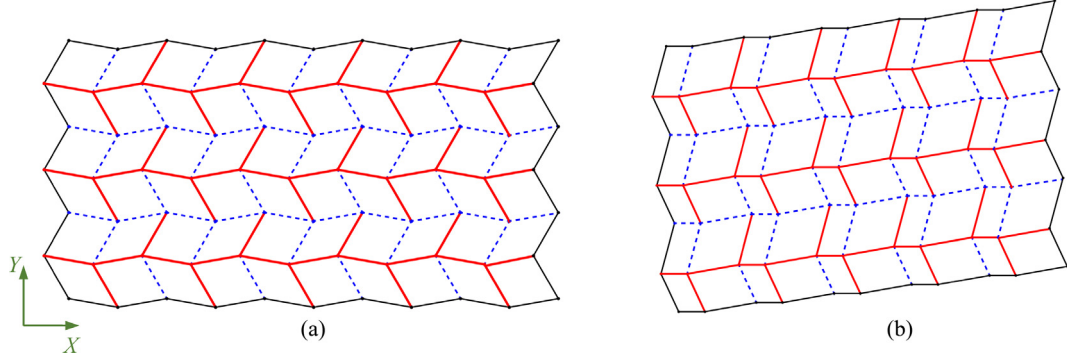
Fig. 5. A valid mountain and valley assignment for the geometric configurations depicted in: (a) Fig. 4(a); (b): Fig. 4(b).

vertices shown in Fig. 4(a) and (b) are different, the assignments of mountain and valley folds are equivalent.

Furthermore, here we study two quadrilateral mesh patterns, namely the Miura and Bellow [43,44] patterns, as shown in Fig. 6, to investigate the performance of the proposed computational scheme.

For the Miura geometric configuration shown in Fig. 6(a), the angles between the bottom two vectors of the vertical subgraph and the X-axis are $\theta_{v1} = 105°$ and $\theta_{v2} = 75°$, respectively, and the lengths of edges along the subgraph are identical. For the Bellow geometric configuration shown in Fig. 6(b), the angles between the bottom two vectors of the even vertical subgraphs and the X-axis are $\theta_{v1} = 75°$ and $\theta_{v2} = 105°$, and the others are similar to those of the Miura geometric configuration shown in Fig. 6(a). The lengths of the adjacent edges of the horizontal subgraph are

l_{u1} and l_{u2}, and the length of each edge of the vertical subgraph is l_v. In fact, the vertical zigzag polylines of the Bellow configuration are reflected about the neighboring ones to allow these lines to be symmetric along the vertical direction.

A total of 60 quadrilateral facets are detected for each structure, where the involved computation time is less than 0.050 s. Subsequently, optimal solutions of the origami structures with the Miura and Bellow patterns are obtained, which cost respectively 0.4315 s and 0.4499 s to implement the automated assignments on mountain and valley folds. The obtained patterns are illustrated in Fig. 7.

The result obtained from the proposed computational method agree well with the well-known mountain-valley assignments of these two patterns. Importantly, as expected, all transverse polylines in the Bellow pattern turned out to be mountain folds. The Miura pattern consists of 55 mountains and 49 valley folds, while
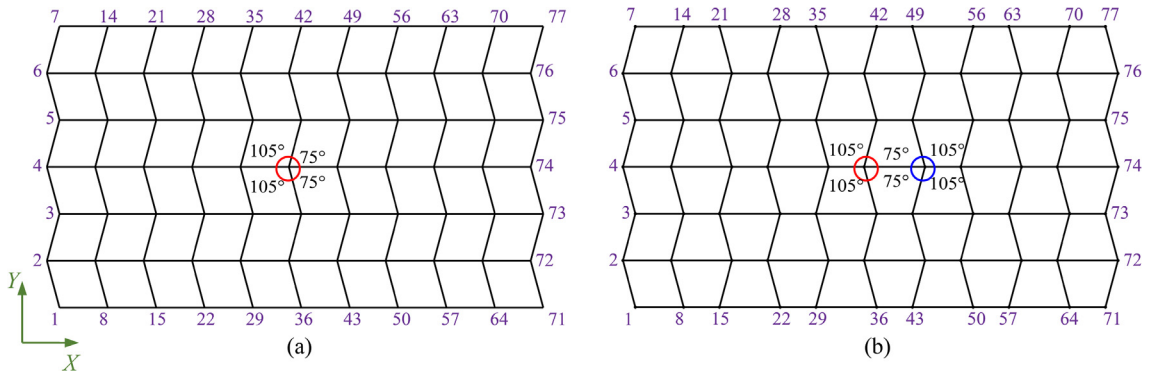

Fig. 6. Geometric configurations of two conventional origami patterns with 11 × 7 vertices: (a) the Miura pattern; (b) the Bellow pattern.
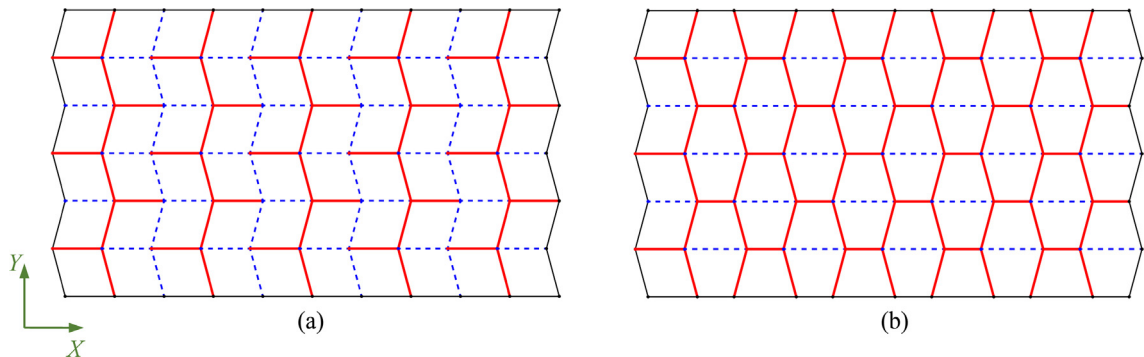

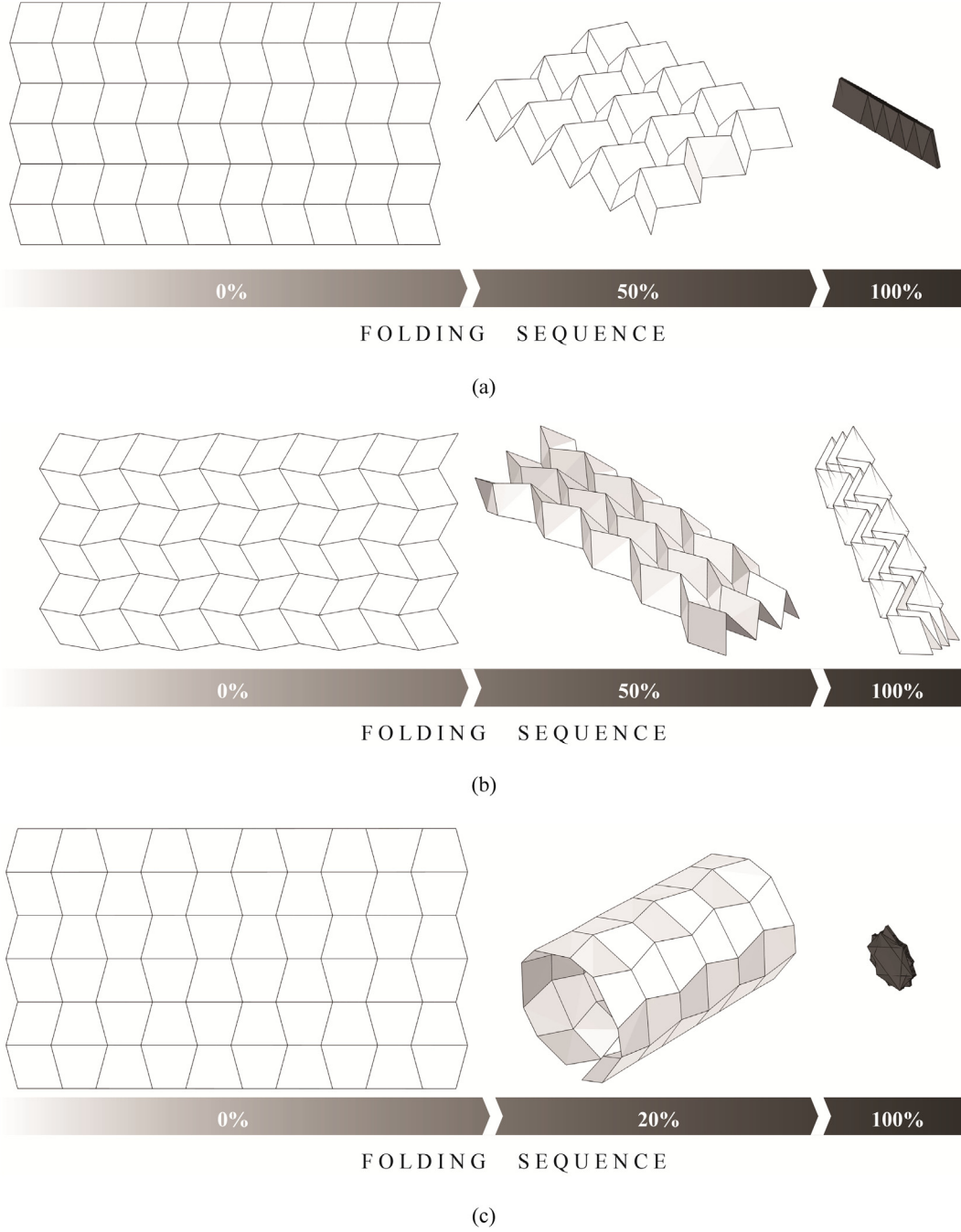**Fig. 7.** Optimal solutions of origami structures with 11 × 7 vertices: (a) the Miura pattern; (b) the Bellow pattern.

Fig. 8. Geometric transformations of origami patterns with 11×7 vertices during flat-folding: (a) the Miura pattern; (b) the $pgg_{2,2}^+$ descendant of the Miura pattern; (c) the Bellow pattern.

the Bellow pattern consists of 79 mountains and 25 valley folds. The folding sequences of the patterns studied in this section are presented in Fig. 8.

4.3. Origami patterns with degree-6 vertices

To investigate whether the proposed method is applicable to crease patterns with degree-6 vertices (i.e., $d = 6$), several patterns with Kresling or Waterbomb patterns are studied in this section. Fig. 9 shows two Kresling fold patterns [26,45], each of which consisting of 7×5 vertices and 82 edges.

Based on the geometric-graph-theoretic approach [28], the two Kresling patterns can be obtained from the Type I directed graph

products of their corresponding directed subgraphs shown in Fig. 9. Then, the adjacency matrix **A** for each of the two patterns can be expressed as

$$\boldsymbol{A}\big(G_1(\times)_I G_2\big) = \mathbf{A}(G_1) \otimes \mathbf{I}_5 + \mathbf{I}_7 \otimes \boldsymbol{A}(G_2) + \bar{\boldsymbol{A}}(G_1) \otimes \bar{\boldsymbol{A}}(G_2)$$
$$+ \bar{\boldsymbol{A}}^T(G_1) \otimes \bar{\boldsymbol{A}}^T(G_2), \tag{31}$$

where $(\times)_I$ denotes the Type I directed graph product [46], $\boldsymbol{A}(G_1)$ and $\boldsymbol{A}(G_2)$ denote the adjacency matrices of undirected graphs of the horizontal subgraph G_1 and the vertical subgraph G_2, respectively; $\bar{\boldsymbol{A}}(G_1)$ and $\bar{\boldsymbol{A}}(G_2)$ represent the modified adjacency matrices of directed subgraphs G_1 and G_2, and $\bar{\boldsymbol{A}}^T$ indicates the transpose of
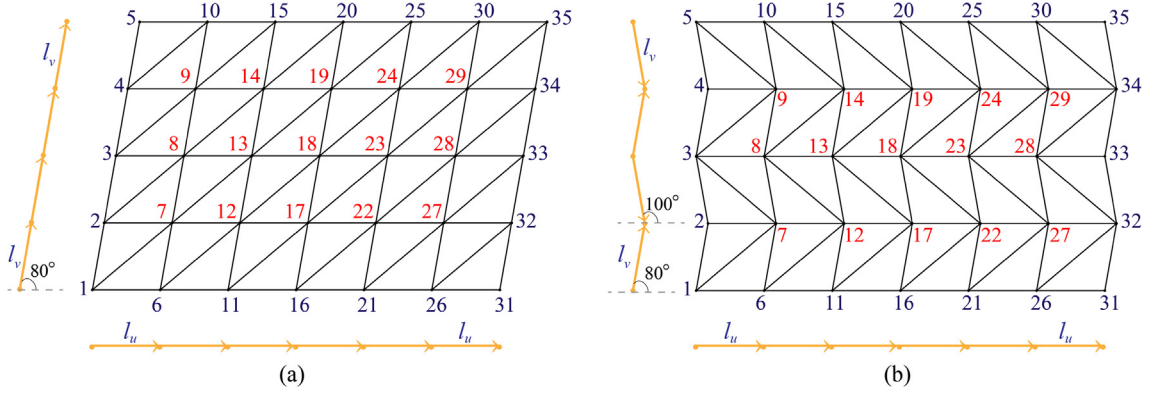
Fig. 9. Two different Kresling origami patterns with degree-6 vertices: (a) a Kresling pattern with inclined symmetry axes (inclinedy-asymmetric); (b) a Kresling pattern with horizontal symmetry axes (horizontally-asymmetric).

matrix $\bar{A}$. As the edges of the subgraph G_1 retain the same direction from left to right, the matrices $A(G_1)$ and $\bar{A}(G_1)$ for both structures are

$$A(G_1) = \begin{bmatrix} 0 & 1 & 0 & 0 & 0 & 0 & 0 \\ 1 & 0 & 1 & 0 & 0 & 0 & 0 \\ 0 & 1 & 0 & 1 & 0 & 0 & 0 \\ 0 & 0 & 1 & 0 & 1 & 0 & 0 \\ 0 & 0 & 0 & 1 & 0 & 1 & 0 \\ 0 & 0 & 0 & 0 & 1 & 0 & 1 \\ 0 & 0 & 0 & 0 & 0 & 1 & 0 \end{bmatrix} \text{ and}$$

$$\bar{A}(G_1) = \begin{bmatrix} 0 & 1 & 0 & 0 & 0 & 0 & 0 \\ 0 & 0 & 1 & 0 & 0 & 0 & 0 \\ 0 & 0 & 0 & 1 & 0 & 0 & 0 \\ 0 & 0 & 0 & 0 & 1 & 0 & 0 \\ 0 & 0 & 0 & 0 & 0 & 1 & 0 \\ 0 & 0 & 0 & 0 & 0 & 0 & 1 \\ 0 & 0 & 0 & 0 & 0 & 0 & 0 \end{bmatrix} \tag{32}$$

For the structure shown in Fig. 9(a), the matrices for the directed subgraph G_2 are

$$A(G_2) = \begin{bmatrix} 0 & 1 & 0 & 0 & 0 \\ 1 & 0 & 1 & 0 & 0 \\ 0 & 1 & 0 & 1 & 0 \\ 0 & 0 & 1 & 0 & 1 \\ 0 & 0 & 0 & 1 & 0 \end{bmatrix} \text{ and } \bar{A}(G_2) = \begin{bmatrix} 0 & 1 & 0 & 0 & 0 \\ 0 & 0 & 1 & 0 & 0 \\ 0 & 0 & 0 & 1 & 0 \\ 0 & 0 & 0 & 0 & 1 \\ 0 & 0 & 0 & 0 & 0 \end{bmatrix}, \tag{33}$$

where the fifth vertex of the vertical subgraph is the ending point. Similarly, the matrices for the subgraph G_2 of the structure shown in Fig. 9(b) are

$$A(G_2) = \begin{bmatrix} 0 & 1 & 0 & 0 & 0 \\ 1 & 0 & 1 & 0 & 0 \\ 0 & 1 & 0 & 1 & 0 \\ 0 & 0 & 1 & 0 & 1 \\ 0 & 0 & 0 & 1 & 0 \end{bmatrix} \text{ and } \bar{A}(G_2) = \begin{bmatrix} 0 & 1 & 0 & 0 & 0 \\ 0 & 0 & 0 & 0 & 0 \\ 0 & 1 & 0 & 1 & 0 \\ 0 & 0 & 0 & 0 & 0 \\ 0 & 0 & 0 & 1 & 0 \end{bmatrix}, \tag{34}$$

where the zero entries along the second and fourth rows describe that the second and fourth vertices are the ending points of the directed subgraph G_2. As can be seen from Fig. 9, the lengths of the horizontal and vertical edges are respectively l_u and l_v. In addition, the angle between the X-axis and the vectors of the vertical

subgraph shown in Fig. 9(a) is 80°, and the two angles between the X-axis and the first two vectors of the vertical subgraph shown in Fig. 9(b) are respectively 80° and 100°.

It takes approximately 0.030 s to detect a total of 48 triangle facets, 62 internal edges, and 15 internal vertices. The set $\bar{V}$ associated with the internal vertices is marked in Fig. 9, given by

$$\bar{V} = [7 \ 8 \ 9 \ 12 \ 13 \ 14 \ 17 \ 18 \ 19 \ 22 \ 23 \ 24 \ 27 \ 28 \ 29]^T \tag{35}$$

It is important to point out that all the internal and boundary edges can be correctly identified by Eqs. (7) and (8). For instance, although a diagonal edge connects the boundary vertices 26 and 32 in Fig. 9(a), it should be an internal edge (not boundary edge). Since all the internal vertices satisfy the local flat-foldability condition, there should be a feasible assignment on the mountain and valley folds to allow the given structures to be flat-foldable. A common property of both patterns is that all the diagonal edges are valley folds, while all other internal edges are mountain folds. Fig. 10 also shows the partially folded configurations of these flat-foldable structures.

Using a mixed-integer linear programing algorithm, we develop feasible and flat-foldable patterns for both the inclinedly-symmetric and horizontally-symmetric Kresling patterns. The corresponding patterns are shown in Fig. 10(a) and (b), for which the computational process takes respectively 0.3982 s and 0.4042 s. Besides, the symmetry of the folded configuration belongs to the subgroups of the symmetry of the intial origami pattern [47–51]. As shown in Fig. 10, the inclinedly-symmetric Kresling pattern retains asymmetric configuration, while the horizontally-symmetric Kresling pattern keeps horizontally-symmetric.

We have also utilized the proposed method to predict the mountain and valley assignments for a much larger-scale Water-bomb origami structure, which consists of 336 vertices and 935 edges (see Fig. 11a). On the basis of the graph-theoretic approach and the cycle detection method, 600 triangle facets, 865 internal edges, and 266 internal vertices are detected within 0.2147 s.

Notably, the proposed method still exhibits a good computational efficiency for such a complex structure, as the involved computation costs only 1.1492 s. The identified mountain and valley assignments are illustrated in Fig. 11(b). Most of the horizontal and vertical edges are mountain folds, while most of the diagonal edges are valley folds. It should be explained that the top and bottom diagonal edges connected to the boundary vertices are assigned as mountain folds, because of insufficient constraints on the boundary vertices. However, it does not affect the global flat-foldability of the structure. As shown in Fig. 11(c)–(d), this origami
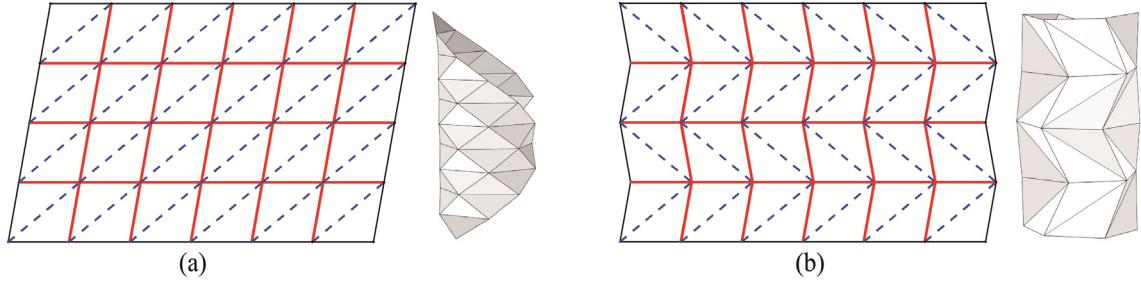
Fig. 10. Obtained patterns with mountain-valley assignments and partially folded configurations for origami structures with degree-6 vertices: (a) the inclinedly-symmetric Kresling pattern; (b) the horizontally-symmetric Kresling pattern.
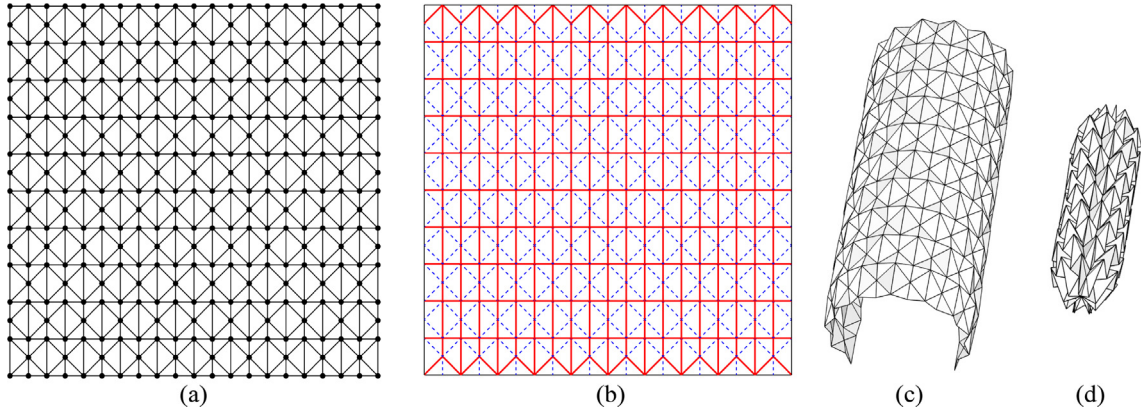

Fig. 11. A Waterbomb origami structure with degree-6 vertices: (a) the given geometric configuration; (b) the pattern with mountain-valley assignments; (c) a partially-folded and (d) the fully-folded structural configurations of the pattern during folding.

structure with Waterbomb pattern gradually transforms from a 2D sheet into a compact and cylindrical structure. In practical design, to guarantee that all the vertices satisfy Theorem 1, we can either add additional boundary vertices to the given geometry, or select the patterns composed by all the internal vertices.

5. Applicability and computational efficiency of the Mountain-Valley assignment method

In this section, the applicability and computational efficiency of the proposed assignment method are discussed. The examples given in Section 4 verified that this method works well for origami patterns with degree-4 and degree-6 vertices. However, further work needs to be carried out in order to develop a robust and comprehensive computational platform for more complex geometric designs such as patterns composed of both degree-4 and degree-6 (and/or degree-8) vertices. Moreover, the proposed method can be potentially improved and integrated to simultaneously evaluate the nodal positions of vertices and mountain-valley assignments of edges.

To further explore the computational efficiency of the proposed method, classical Miura origami structures with $n \times n$ vertices are taken as the input configurations. Similar to those of the Miura structure shown in Fig. 1, the geometric parameters for the given
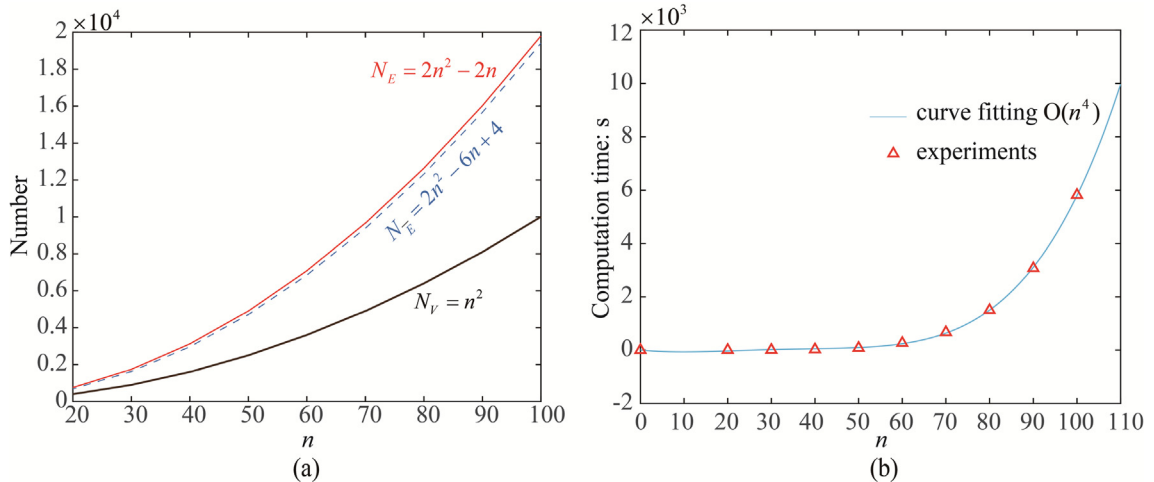

Fig. 12. Computational results for Miura origami patterns with $n \times n$ vertices: (a) number of vertices, internal edges and edges; (b) computation time (seconds).
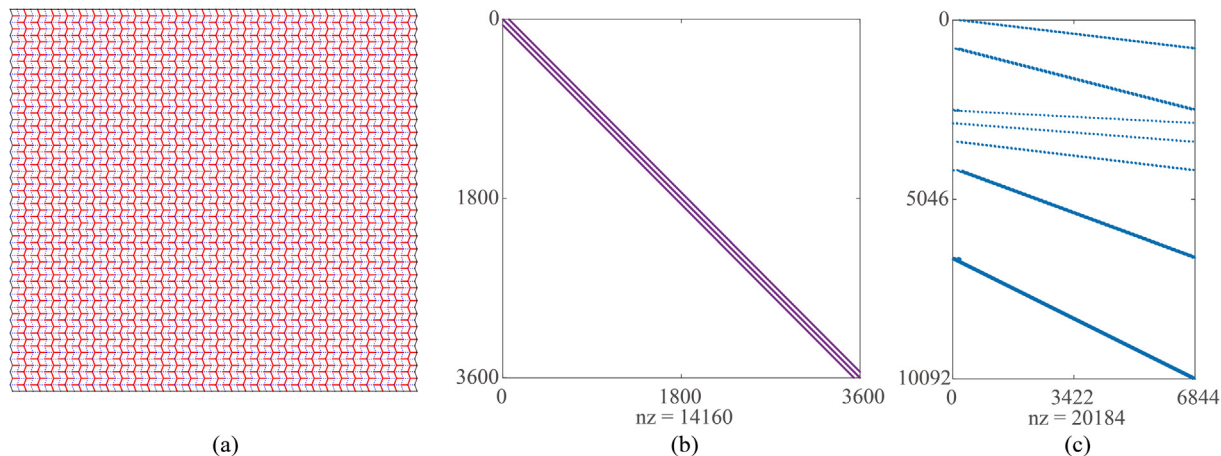
Fig. 13. A classical Miura origami structure with 60 × 60 vertices: (a) mountain and valley assignments; (b) distribution pattern of nonzero entries of the adjacency matrix **A**; (c) distribution pattern of nonzero entries of the compatibility matrix for the constraints.

structures are $l_u = l_v$, $\theta_{u1} = \theta_{u2} = 0°$, $\theta_{v1} = 120°$, and $\theta_{v2} = 60°$. Fig. 12(a) shows the total number of vertices N_V, the number of edges N_E, and the number of internal edges $N_{\bar{E}}$, substantially affected by the rising value of n. As can be seen from the figure, the curves exhibit quadratic growths.

It turns out that our method is capable of automated and stable identification of valid mountain and valley folds for any given structure, regardless of the variation of n. As shown in Fig. 12(b), the computational cost of the proposed method is considerably dependent on the number of vertices. Any origami structure satisfying the local flat-foldability constraints of its $n \times n$ vertices has a valid assignment of mountain and valley folds, computable in approximately O(n^4) time.

For instance, Fig. 13 shows the obtained origami pattern and distribution patterns of the involved matrices for the origami structure with 60 × 60 vertices. Although this structure consists of as many as 3600 vertices and 7080 edges, the optimal solution for the mountain and valley folds is obtained within 260.6531 s. However, for the origami structure with 100 × 100 vertices, the corresponding origami design is computationally expensive, taking up 5817.7962 s for the whole computational process. In fact, since the structures show strong regularity (see Fig. 13a), their inherent symmetry or periodicity can be utilized to simplify the practical design process. On the other hand, as the involved matrices are large-sized sparse matrix (see Fig. 13b and c), storage and computing methods for sparse matrices are helpful to further improve the computational efficiency.

6. Conclusions

This study presented a computational method for assigning mountain and valley folds to given geometric configurations of origami crease patterns. The method is based upon a geometric-graph-theoretic representation approach combined with a cycle detection algorithm using graph theory, which does not require the connectivity of edges or facets to be given in advance. The original design problem is converted to a mixed-integer linear programming problem. Three parameters for the edges are adopted to generate valid and flat-foldable origami patterns from a given initial geometric configuration. Several constraints are employed to implicitly guarantee the degree of each vertex and the opposition of fold lines associated with local minimum angles. In conjunction with the objective function that minimizes the number of valley folds, the upper bound for the fold lines serves as a measure of the total number of edges of the given structure.

A range of examples demonstrated that the mountain-valley assignments for various origami patterns can be obtained from the subgraphs associated with the edges and the degree of the vertices of the initial geometric configuration. The proposed design method is implementable in approximately O(n^4) time, where n is the maximum number of vertices of the subgraphs. In particular, we showed that the proposed approach is appropriate for developing origami patterns with degree-4 or degree-6 vertices, which are currently most common in origami engineering. In the future, we will further develop the numerical method to be applied to geometric configurations composed of vertices with different degrees, enabling the automated design of more complex origami structures.

Declaration of Competing Interest

The authors declare that they have no known competing financial interests or personal relationships that could have appeared to influence the work reported in this paper.

References

[1] Lang RJT. Complete book of origami: step-by-step instructions in over 1000 diagrams: 37 original models. Dover Pubns 2013.
[2] Rivas-Adrover E. A new hybrid type of deployable structure: origami-scissor hinged. J Int Assoc Shell Spatial Struct 2018;59(3):183–90.

[3] Sorguç AG, Hagiwara I, Selcuk S. Origamics in architecture: a medium of inquiry for design in architecture. Metu Jfa 2009;2:235–47.

[4] Nishiyama Y. Miura folding: applying origami to space exploration. Osaka Keidai Ronshu 2009;60(1):17–24.

[5] Chen Y, Feng J. Folding of a type of deployable origami structures. Int J Struct Stab Dyn 2012;12(6):1250054.

[6] Chen Y, Yan J, Feng J, Sareh P. PSO-based metaheuristic design generation of non-trivial flat-foldable origami tessellations with degree-4 vertices. Journal of Mechanical Design-Transactions of the ASME 2020:1–25. https://doi.org/10.1115/1.4047437.

[7] Sareh P, Chermprayong P, Emmanuelli M, Nadeem H, Rotorigami KM. A rotary origami protective system for robotic rotorcraft. Sci Robot 2018;3(22): eaah5228.

[8] Hunt GW, Ario L. Twist buckling and the foldable cylinder: an exercise in origami. Int J Non Linear Mech 2005;40(6):833–43.

[9] Kuribayashi K, Tsuchiya K, You Z, Tomus D, Umemoto M, Ito T, Sasaki M. Self-deployable origami stent grafts as a biomedical application of Ni-rich TiNi shape memory alloy foil. Mater Sci Eng A – Struct Mater Properties Microstruct Process 2006;419(1–2):131–7.

[10] Silverberg JL, Jun-Hee N, Evans AA, Bin L, Hull TC, Santangelo CD, Lang RJ, Hayward RC, Itai C. Origami structures with a critical transition to bistability arising from hidden degrees of freedom. Nat Mater 2015;14(4):389–93.

[11] Yang J, Yasuda H. Reentrant origami-based metamaterials with negative poisson's ratio and bistability. Phys Rev Lett 2015;114(18):185502.

[12] Fang H, Chu SCA, Xia Y, Wang KW. Programmable self-locking origami mechanical metamaterials. Adv Mater 2018;30(15):1706311.

[13] Zhai Z, Wang Y, Jiang H. Origami-inspired, on-demand deployable and collapsible mechanical metamaterials with tunable stiffness. Proc Natl Acad Sci 2018;115(9):2032–7.

[14] Li S, Fang H, Sadeghi S, Bhovad P, Wang KW. Architected origami materials: How folding creates sophisticated mechanical properties. Adv Mater 2019;31 (5):1805282.

[15] Demaine ED, O'Rourke J. Geometric folding algorithms: linkages, origami, polyhedra. New York: Cambridge University Press; 2007.

[16] Lang RJ. Twists, tilings, and tessellations: mathematical methods for geometric origami. Boca Raton, FL: CRC Press; 2018.

[17] Belcastro SM, Hull TC. Modelling the folding of paper into three dimensions using affine transformations. Linear Algebra Appl 2002;348:273–82.

[18] Tachi T. Generalization of rigid foldable quadrilateral mesh origami. J Int Assoc Shell Spatial Struct 2009;50(162):173–9.

[19] Zhou X, Wang H, You Z. Design of three-dimensional origami structures based on a vertex approach. Proc R Soc A 2015;471(2181):20150407. https://doi.org/10.1098/rspa.2015.0407.

[20] Qiu C, Zhang K, Dai JS. Repelling-screw based force analysis of origami mechanisms. J Mech Robot-Trans ASME 2016;8(3):031001.

[21] Wei G, Dai JS. Origami-inspired integrated planar-spherical overconstrained mechanisms. J Mech Des-Trans ASME 2014;136(5):051003.

[22] Fuchi K, Diaz AR. Origami design by topology optimization. J Mech Des-Trans ASME 2013;135(11):111003.

[23] Zimmermann L, Stanković T. Rigid and flat foldability of a degree-four vertex in origami. J Mech Robot-Trans ASME 2020;12(1):011004.

[24] McAdams DA, Li W. A novel method to design and optimize flat-foldable origami structures through a genetic algorithm. J Comput Inform Sci Eng-Trans ASME 2014;14(3):031008.

[25] Sareh P. The least symmetric crystallographic derivative of the developable double corrugation surface: computational design using underlying conic and cubic curves. Mater Des 2019;108128.

[26] Sareh P. Symmetric descendants of the Miura-ori. UK: University of Cambridge; 2014.

[27] Sareh P, Guest SD. Design of isomorphic symmetric descendants of the Miura-ori. Smart Mater Struct 2015;24(8):085001.

[28] Chen Y, Sareh P, Yan J, Fallah AS, Feng J. An integrated geometric-graph-theoretic approach to representing origami structures and their corresponding truss frameworks. J Mech Des-Trans ASME 2019;141(9):091402.

[29] Chen Y, Fan L, Feng J. Kinematic of symmetric deployable scissor-hinge structures with integral mechanism mode. Comput Struct 2017;191:140–52.

[30] Hull TC. Counting mountain-valley assignments for flat folds. arXiv preprint arXiv:1410.5022 2014.

[31] Ehara S, Kanno Y. Topology design of tensegrity structures via mixed integer programming. Int J Solids Struct 2010;47(5):571–9.

[32] Xu X, Wang Y, Luo Y. Finding member connectivities and nodal positions of tensegrity structures based on force density method and mixed integer nonlinear programming. Eng Struct 2018;166:240–50.

[33] Hull T. On the mathematics of flat origamis. Congressus numerantium 1994:215–24.

[34] On KT. the relation between mountain-creases and valley-creases of a flat origami. Proceedings of the first international meeting of origami science and technology, 1991.

[35] Chen Y, Yan J, Sareh P, Feng J. Feasible prestress modes for cable-strut structures with multiple self-stress states using particle swarm optimization. J Comput Civil Eng 2020;34(3):04020003.

[36] Chen Y, Feng J. Generalized eigenvalue analysis of symmetric prestressed structures using group theory. J Comput Civil Eng 2012;26(4):488–97.

[37] Chen Y, Sareh P, Feng J, Sun Q. A computational method for automated detection of engineering structures with cyclic symmetries. Comput Struct 2017;191:153–64.

[38] Kaveh A. Optimal analysis of structures by concepts of symmetry and regularity. Wien-NewYork: Springer Verlag, GmbH; 2013.

[39] Boukerche A, Tropper C. A distributed graph algorithm for the detection of local cycles and knots. IEEE Trans Parallel Distrib Syst 1998;9(8):748–57.

[40] Mou B, Bai Y, Patel V. Post-local buckling failure of slender and over-design circular CFT columns with high-strength materials. Eng Struct 2020;210:110197.

[41] Hu J, Chen W, Qu Y, Yang D. Safety and serviceability of membrane buildings: A critical review on architectural, material and structural performance. Eng Struct 2020;110292.

[42] Hu J, Kawaguchi K, Ma J. Long-term building thermal performance of enclosed large-span swimming stadiums with retractable membrane ceilings. Energy Build 2019;109363.

[43] Reid A, Lechenault F, Rica S, Adda-Bedia M. Geometry and design of origami bellows with tunable response. Phys Rev E 2017;95(1):013002.

[44] Yasuda H, Yein T, Tachi T, Miura K, Taya M. Folding behaviour of Tachi–Miura polyhedron bellows. Proc R Soc A 2013;469(2159):20130351. https://doi.org/10.1098/rspa.2013.0351.

[45] Guest SD, Pellegrino S. The folding of triangulated cylinders. Part II. The folding process. J Appl Mech-Trans ASME 1994;61(4):778–83.

[46] Kaveh A, Koohestani K. Graph products for configuration processing of space structures. Comput Struct 2008;86(11):1219–31.

[47] Chen Y, Yan J, Sareh P, Feng J. Nodal flexibility and kinematic indeterminacy analyses of symmetric tensegrity structures using orbits of nodes. Int J Mech Sci 2019;155:41–9. https://doi.org/10.1016/j.ijmecsci.2019.02.021.

[48] Zingoni A. On the best choice of symmetry group for group-theoretic computational schemes in solid and structural mechanics. Comput Struct 2019;223:106101.

[49] Chen Y, Feng J, Sun Q. Lower-order symmetric mechanism modes and bifurcation behavior of deployable bar structures with cyclic symmetry. Int J Solids Struct 2018;139–140:1–14.

[50] Chen Y, Sareh P, Feng J. Effective insights into the geometric stability of symmetric skeletal structures under symmetric variations. Int J Solids Struct 2015;69–70:277–90.

[51] Sareh P, Chen Y. Intrinsic non-flat-foldability of two-tile DDC surfaces composed of glide-reflected irregular quadrilaterals. Int J Mech Sci 2020;185:105881. https://doi.org/10.1016/j.ijmecsci.2020.105881.